Accurate and dynamic 3D shape measurement with DIC-assisted phase shifting

Pengyu Hu[1], Shuming Yang[1], Fenghe Zheng[1], Ye Yuan[1], Teng Wang[1], Shusheng Li[1], Haibao Liu[2] and John P. Dear[2]

[1] State Key Laboratory for Manufacturing Systems Engineering, Xi'an Jiaotong University, Xi'an, Shaanxi, China
[2] Department of Mechanical Engineering, Imperial College London, London SW7 2AZ, United Kingdom

E-mail: shuming.yang@mail.xjtu.edu.cn

Abstract

Phase shifting profilometry (PSP) has been widely used in structured-light (SL) system for three-dimensional (3D) shape measurements, but the speed of PSP technique is limited by the increased phase-shifting patterns. This paper proposes an accurate and dynamic 3D shape measurement method by projecting only four patterns including three-step phase-shifting patterns and one speckle pattern. Three-step phase-shifting images are used to obtain the initial unwrapped phase map with phase ambiguity. Based on the principle of digital image correlation (DIC) and multi-view geometry, the absolute phase can be recovered reliably without requiring any embedded features or pre-defined information of the object. To improve the measurement accuracy, the projector coordinate is used as the measuring coordinate to establish a novel stereo structured-light system model. By solving a least square solution using the triple-view information, accurate 3D surface data can be reconstructed. The experimental results indicate that the proposed method can perform high-speed and accurate 3D shape measurements with an accuracy of 10.64 μm, which is superior to conventional methods and has certain instructive significance for 3D profilometry and measurement engineering.

Keywords: 3D shape measurement, structured-light, phase shifting profilometry, digital image correlation, stereo vision

1. Introduction

Optical three-dimensional (3D) measurement technology has been widely used in industrial manufacturing, biomedical engineering and reverse engineering due to its high precision, high efficiency, and non-contact characteristics [1]. It can be classified into active methods and passive methods depending on whether projecting the light filed or not. Typical passive methods, including photogrammetry [2], binocular vision [3] and multi-view stereo vision [4], realize 3D sensing by matching the feature points in the images. These passive methods are limited by the texture of scenes and have a lower accuracy compared to the active methods, which include time-of-flight [5], laser scanning [6], structured-light (SL) [7] and optical interferometry [8]. As one of the typical active methods, the SL method projects a series of encoded patterns to the object. By decoding the SL patterns modulated by the surface of the object, accurate and efficient 3D data can be acquired using the principle of stereo vision.

Many SL codification methods, including random encoding methods [9], binary encoding methods [10] and sinusoidal phase encoding methods [11], have been developed in the past few decades. One unique advantage of random encoding methods is that only a single pattern needs to be projected and 3D measurement can be easily realized using digital image correlation (DIC) technique [12] , but the spatial

resolution and accuracy of random encoding methods is relatively low due to the limitation of random features encoding resolution. Compared to random encoding methods, phase encoding methods can perform measurements with higher resolution and better accuracy 3D. Amongst those phase encoding methods, the phase shifting profilometry (PSP) [13] has been widely used due to its robustness to the environment. To acquire a full-filed continuous phase distribution in PSP, phase unwrapping is a necessary procedure, which can be classified into spatial phase unwrapping and temporal phase unwrapping. The spatial phase unwrapping methods [14] can only produce relative phase map by checking surrounding pixels and removing the 2π discontinuities, which induces phase ambiguities and could fail for the measurements of multiple isolated surfaces. Temporal phase unwrapping methods, represented by the multi-frequency method [15] and the Gray-code [16] method, can obtain the absolute phase distribution of complex scenes, but the speed of PSP is limited by the increased patterns.

Considering that the speed of PSP is negatively related to the number of patterns, the challenge of performing high-speed PSP is to recover the absolute phase using fewer patterns. Cong et al. [17] proposed a parallel spatial unwrapping strategy by embedding a sparse set of markers in three-step phase shift patterns and solved the problem of phase ambiguity. Stereo-assisted phase shifting method [18] was also presented to perform absolute 3D measurement. But the process of rejecting the wrong candidates could fail in textureless area and the depth range is required to be pre-defined, which is not robust in practical application. Pixel-wise phase unwrapping methods [19, 20], using geometric constraints, have also been developed, which do not require any additional images, markers or cameras, but the phase unwrapping quality may relate to the virtual Z_{min} plane. Wu et al. [21] proposed a variant shifting-phase method to retrieve the absolute phase by embedding the code-word of the fringe order into a shifting-phase term, while the precision of phase unwrapping may be easily affected by the quality of pixels, especially in some area with a low signal to noise ratio.

To reduce the number of SL patterns while retaining the quality of phase map, SL methods based on the combination of DIC technique and fringe projection technique have been proposed in the past few years. These methods can be divided into two categories: composite patterns projection [22–23] and combined patterns projection [24, 26]. The composite patterns projection methods generally embed the speckle pattern into phase shifting patterns to solve the problem of phase ambiguities. Lohry et al. [23] proposed a stereo SL system using speckle-embedded three-step phase shifting patterns, which first obtains a coarse disparity map by stereo matching followed by refining the coarse disparity using wrapped phase. This method omits the phase unwrapping process, but the embedded speckle will substantially compromise the phase modulation and decrease the measurement accuracy. On this basis, Yin et al. [24] proposed a high-speed stereo SL system based on an optimized speckle embedding method. Using the pre-defined depth range and DIC technique, the periodic phase ambiguities can be ruled out. This method decreases the impact of embedded speckle on sinusoidal phase codewords to some extent, but it still suffers from low quality and low robustness when measuring complex surfaces. The combined patterns projection methods use an additional speckle pattern to eliminate the phase ambiguities of PSP using stereo geometry constraints and can retain the performance of PSP. Gai et al. [25] developed a stereo SL system based on the combined projection of four-step phase-shifting patterns and one speckle pattern. Similar to reference [23], this method firstly calculates the initial matching information using speckle pattern and then refines the initial matching results using the wrapped phase data. While the initial matching results contains substantial errors, which will bring difficulties to the subsequent matching refinement, and the pixel-by-pixel correlation increases the computation cost. Feng et al. [26] combined three-step phase shifting patterns with one speckle pattern to solve the phase unwrapping problem in stereo SL system. This method can produce an absolute phase map, but in the process of calculating 3D coordinates, the information of stereo images is underutilized, which limits the measurement accuracy.

To improve the speed of PSP system while retaining high precision, this paper presents an accurate and dynamic 3D shape measurement method based on DIC-assisted phase shifting and stereo SL system model, which only needs to project four patterns including three-step phase-shifting patterns and one speckle pattern. Three-step phase-shifting images are used to obtain the initial unwrapped phase map with phase ambiguity. Based on the principles of DIC and stereo vision using the speckle images, full-field continuous phase map can be obtained. To make the best use of the stereo cameras, the projector coordinate is used as the measuring coordinate and the stereo SL system model is proposed. By calculating a least square solution using the triple-view information, more accurate 3D surface data can be reconstructed. Compared with the related works [17–26], the proposed method makes adequate use of triple-view information to achieve more accurate 3D measurement with relative less computational correlation cost, which has certain instructive significance in the field of 3D profilometry and practical measurement engineering.

2. Principles

2.1. Three-step phase-shifting algorithm

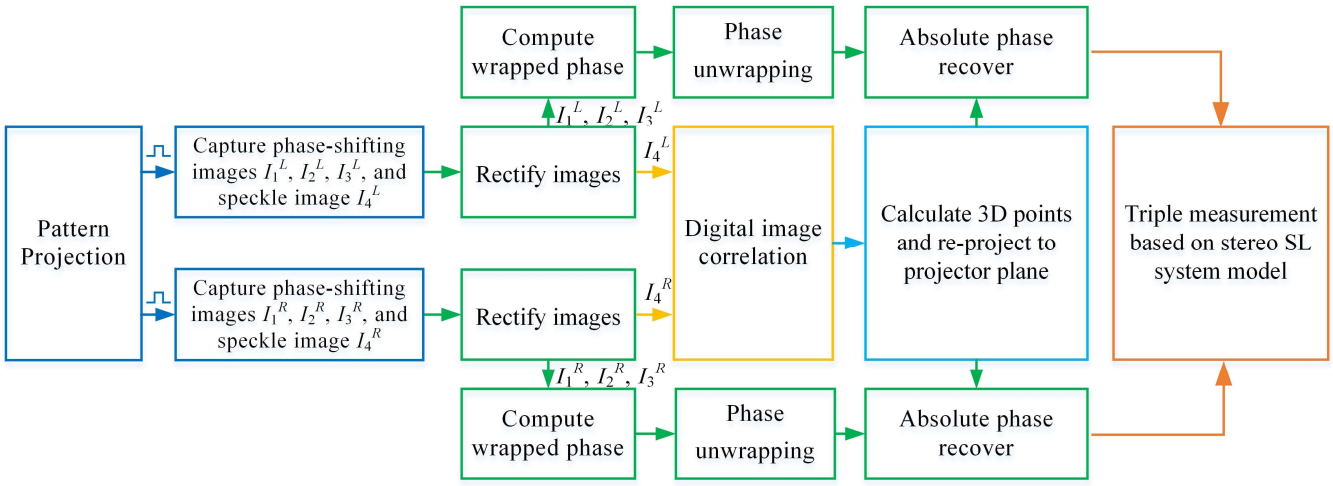

Figure 1. The flowchart of DIC-assisted phase-shifting method using stereo SL system model.

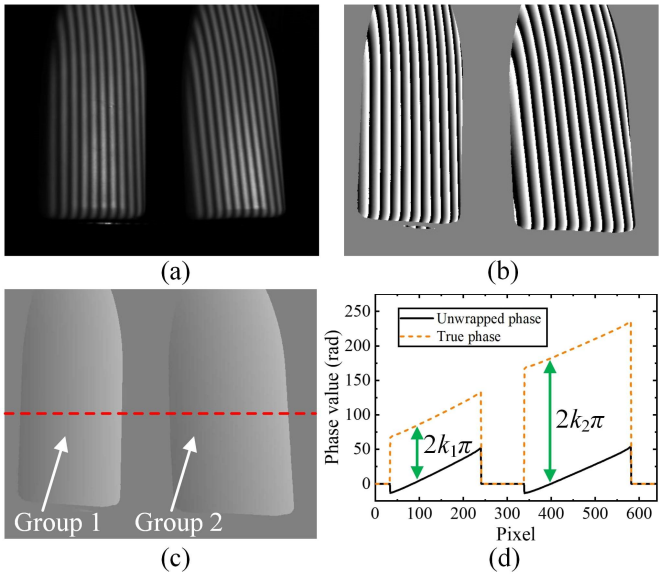

Figure 2. (a) First frame of three-step phase shift images. (b) Wrapped phase map. (c) Unwrapped phase map containing two phase groups. (d) One cross section (red dash line in (c)) of unwrapped phase map.

Three-step phase-shifting algorithm is suitable for high-speed measurements due to its advantage of requiring the minimum number of patterns for phase extraction. By the three-step phase-shifting algorithm, the intensities of the patterns can be described as follows:

$$I_1(x,y) = A(x,y) + B(x,y)\cos(\varphi(x,y)), \quad (1)$$

$$I_2(x,y) = A(x,y) + B(x,y)\cos(\varphi(x,y) + 2\pi/3), \quad (2)$$

$$I_3(x,y) = A(x,y) + B(x,y)\cos(\varphi(x,y) + 4\pi/3), \quad (3)$$

where $A(x,y)$ is the average intensity, $B(x,y)$ is the intensity modulation, $\varphi(x,y)$ is the phase to be solved and can be calculated by equation (4):

$$\varphi(x,y) = \arctan\left(\frac{\sqrt{3}(I_3 - I_2)}{2I_1 - I_2 - I_3}\right), \quad (4)$$

The wrapped phase value $\varphi(x,y)$ ranges from $-\pi$ to π due to the arctangent function. In order to remove the 2π discontinuities in the wrapped phase map, a phase unwrapping algorithm is needed. Lei et al. [27] proposed an efficient quality guided path algorithms based on histogram processing of reliability, which is robust to random noise. It should be noted that the obtained wrapped phase is generally required to be compensated using LUT technqiue [28] to elinimate the γ nonlinear error of SL system in practical measurement.

2.2. DIC-assisted absolute phase retrieval

3D-DIC technique can perform 3D reconstruction with relative low accuracy and spatial resolution due to the limitation of correlation window size, but it is adequate to provide sparse correspondence information. Thus, DIC-assisted phase-shifting method is presented to retrieve the absolute phase maps of stereo images using the sparse correspondence provided by DIC technique. The flowchart of the proposed method is shown in figure 1.

First, the projector projects three-step phase-shifting patterns and one speckle pattern onto the object and four images are captured by each camera. Next, three-step phase-shifting images are used to calculate the wrapped phase based on three-step phase-shifting algorithm, which is then unwrapped utilizing the quality guided path algorithm [27]. Figure 2 shows the phase unwrapping result of two isolated objects. There are two isolated phase regions in the left unwrapped phase map, as shown in figure 2(c). The pixels in

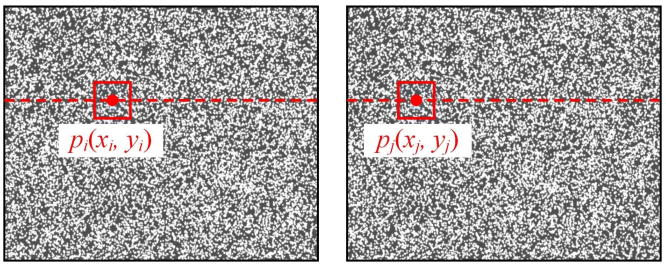

Figure 3. Schematic diagram of DIC.

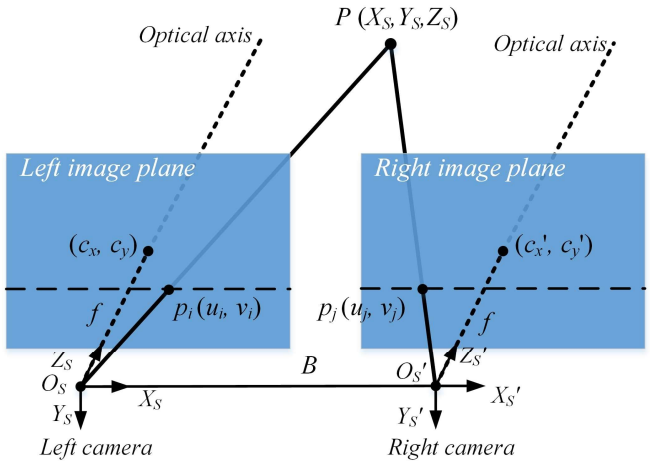

Figure 4. Schematic diagram of stereo vision.

each phase region are considered in one group and each group has an unknown $2k\pi$ phase offset, as shown in figure 2(d). Then, in each group of the left unwrapped phase map, a number of pixels $M = \{p_1, p_2, \cdots, p_n\}$ are randomly sampled. Since the speckle pattern is locally unique, for each sampling pixel $p_i(u_i, v_i)$ in the left speckle image, the corresponding pixel $p_j(u_j, v_j)$ in the right speckle image can be found by searching and calculating the similarity of sub-images centered at $p_i(u_i, v_i)$ and $p_j(u_j, v_j)$, as shown in figure 3, which can be expressed by:

$$R = \frac{\sum_{w=-W}^{W}\sum_{h=-H}^{H} I_l(u_i+w, v_i+h) I_r(u_j+w, v_j+h)}{\sqrt{\sum_{w=-W}^{W}\sum_{h=-H}^{H}\left[I_l(u_i+w, v_i+h)\right]^2 \sum_{w=-W}^{W}\sum_{h=-H}^{H}\left[I_r(u_j+w, v_j+h)\right]^2}}, \tag{5}$$

where $I_l(u, v)$ and $I_r(u, v)$ are the intensity of points (u, v) in the left and right speckle images, respectively, $(2W+1) \times (2H+1)$ is the size of the correlation window, and R is the correlation coefficient, which ranges within [0, 1]. The higher R value represents for higher similarity. Since the stereo images have been rectified, each corresponding point $p_j(u_j, v_j)$ is considered to have the same row index with $p_i(u_i, v_i)$, which can reduce two-dimensional search to one-dimension search. In addition, a correlation threshold is set to ensure the image correlation accuracy.

After the point pair (p_i, p_j) is obtained, based on the principle of stereo vision, as shown in figure 4, the corresponding 3D point $P_s(X_s, Y_s, Z_s)$ of point pair (p_i, p_j) can be calculated by:

$$Z_s = \frac{B \bullet f}{-\left[d - (c_x - c_x')\right]}, \; X_s = \frac{Z_s(u_i - c_x)}{f}, \; Y_s = \frac{Z_s(v_i - c_y)}{f}, \tag{6}$$

where B is the baseline, f is the focal length, and (c_x, c_y) is the optical center of left camera. 3D point $P_s(X_s, Y_s, Z_s)$ is calculated in the rectified left camera coordinate $O_S X_S Y_S Z_S$, which can be expressed as:

$$[X_S, Y_S, Z_S, 1]^T = T_{Rl} \bullet [X_L, Y_L, Z_L, 1]^T, \tag{7}$$

where T_{Rl} is the rectified rotational matrix of the left camera. As shown in figure 5, the left camera coordinate $O_L X_L Y_L Z_L$ is rectified and transformed into $O_S X_S Y_S Z_S$ by the rotational matrix T_{Rl}, and the transformation from projector coordinate $O_P X_P Y_P Z_P$ to left camera coordinate $O_L X_L Y_L Z_L$ can be expressed as:

$$[X_L, Y_L, Z_L, 1]^T = T_{proj\_to\_camL} \bullet [X_P, Y_P, Z_P, 1]^T, \tag{8}$$

3D point $P_s(X_s, Y_s, Z_s)$ in coordinate $O_S X_S Y_S Z_S$ can be transformed into projector coordinate $O_P X_P Y_P Z_P$ and re-projected into the projector image plane by equations (9) and (10):

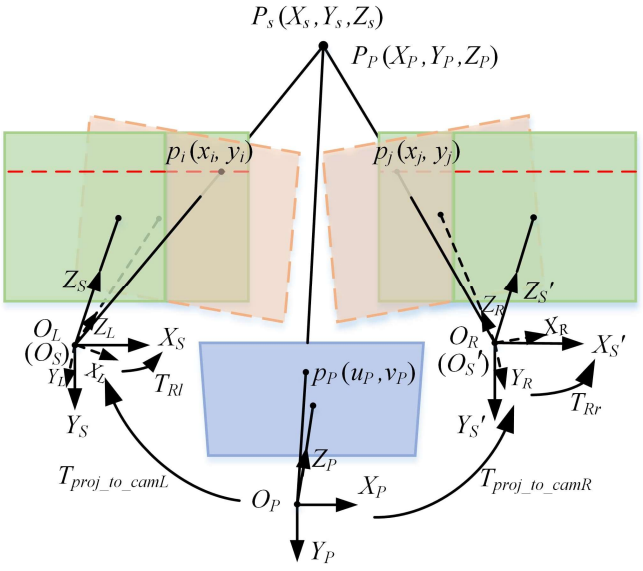

Figure 5. Schematic diagram of stereo SL system model.

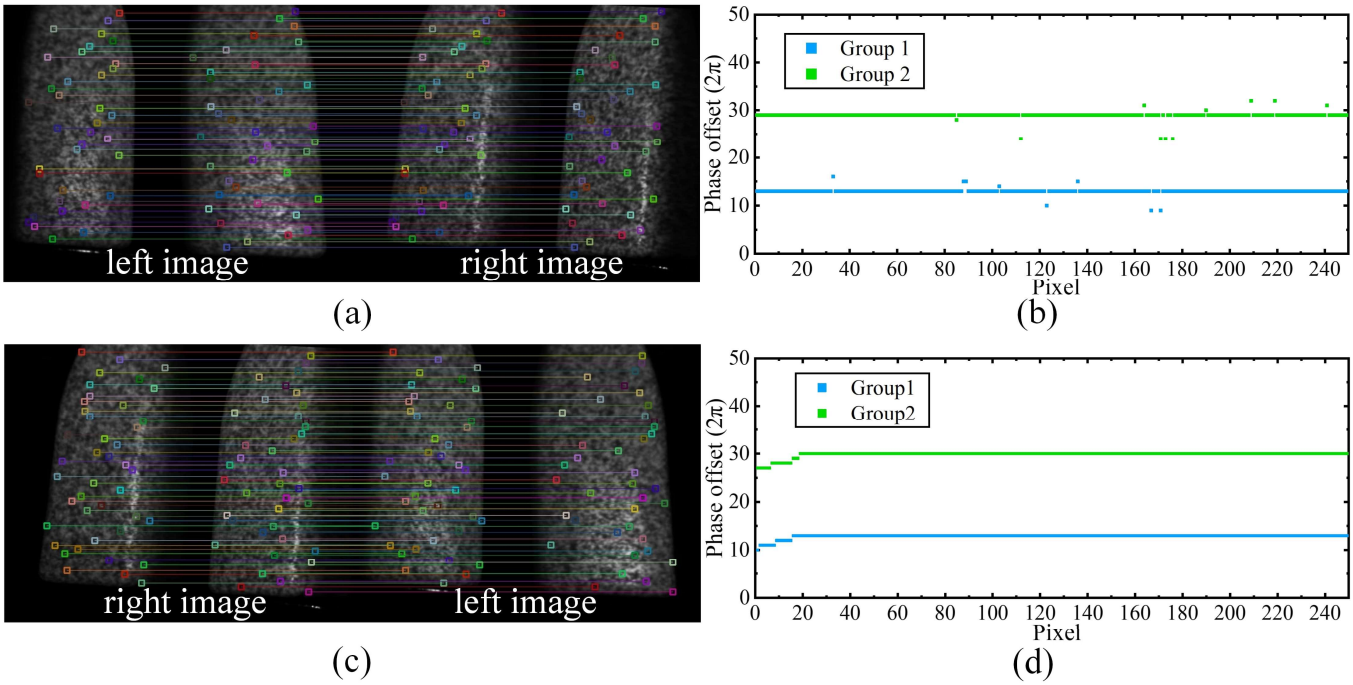

Figure 6. (a) Matching result of partial sampling pixels in the speckle image of left camera. (b) Phase offsets of the sampling pixels in the phase map of left camera. (c)–(d) Corresponding results of right camera.

$$\left[X_P, Y_P, Z_P, 1\right]^T = T_{proj\_to\_camL}^{-1} \bullet T_{Rl}^{-1} \bullet \left[X_S, Y_S, Z_S, 1\right]^T, \quad (9)$$

$$Z_P \left[u_P, v_P, 1\right]^T = P_{proj} \bullet \left[X_P, Y_P, Z_P, 1\right]^T, \quad (10)$$

where P_{proj} is the projection matrix of the projector and (u_p, v_p) is the pixel point in the projector image plane. The matrices $T_{proj\_to\_camL}$, T_{Rl} and P_{proj}, can be acquired by stereo SL system calibration.

Then, the absolute phase value φ_i at point $p_p(u_p, v_p)$ can be calculated by:

$$\varphi_i = \frac{2\pi f}{w} u_p, \quad (11)$$

where f is the cycle number of the phase-shifting fringe and w is the image width of the phase-shifting pattern. Since p_i, p_j and p_p correspond to the same 3D point, the phase value at the three points are equal and the phase offset period k_i of point p_i can be obtained by:

$$k_i = Round\left(\left(\varphi_i - \varphi_i'\right)/\left(2\pi\right)\right), \; i = 1, 2, ..., n \quad (12)$$

where φ_i' is the initial unwrapped phase with ambiguity at point p_i. Due to the image matching error, the phase offset period k_i of each point in $M = \{p_1, p_2, \cdots, p_n\}$ will not be completely the same. Therefore, the k value that appears most frequently is considered to be the true phase offset of the group, which can be expressed as:

$$k = \text{mode}\left(k_1, k_2, ..., k_n\right), \quad (13)$$

The same process is done for the speckle image and unwrapped phase map of right camera. Figures 6(a) and 6(c) show the matching results of partial sampling pixels in the speckle images of left and right cameras, respectively. As shown in figures. 6(b) and 6(d), the phase offsets of group 1 and group 2 are 26π and 58π in the unwrapped phase map of left camera, and 26π and 60π in the unwrapped phase map of right camera, respectively. Subsequently, the absolute phase maps of stereo images can be recovered.

2.3. Stereo structured-light system model

With the absolute phase maps of stereo cameras, the 3D data can be obtained based on the SL system model proposed by Zhang et al. [29], which is described as:

$$s_c \begin{bmatrix} u_c & v_c & 1 \end{bmatrix}^T = P_{cam} \bullet T_{world\_to\_cam} \bullet \begin{bmatrix} X_W & Y_W & Z_W & 1 \end{bmatrix}^T, \quad (14)$$

$$s_p \begin{bmatrix} u_p & v_p & 1 \end{bmatrix}^T = P_{proj} \bullet T_{world\_to\_proj} \bullet \begin{bmatrix} X_W & Y_W & Z_W & 1 \end{bmatrix}^T, \quad (15)$$

$$u_p = \Phi / (2\pi f), \quad (16)$$

where P_{cam} and P_{proj} are the projection matrices of the left camera and the projector, respectively, $T_{world\_to\_cam}$ and $T_{world\_to\_proj}$ are the transformation matrices from the 3D

world coordinate $O_W X_W Y_W Z_W$ to the camera coordinate and the projector coordinate, Φ is the phase value at pixel point (u_c, v_c), and f is the cycle number of the phase-shifting fringe. The matrices P_{cam}, P_{proj}, $T_{world\_to\_cam}$ and $T_{world\_to\_proj}$ can be acquired after SL system calibration. But the SL system model is not suitable for stereo SL system due to the following limitations:

(1) Random error. The 3D world coordinate is considered as the measurement coordinate, which is established on the calibration board. In the process of system calibration, the 3D world coordinate is changing with the position of calibration board, and the transformation matrices $T_{world\_to\_cam}$ and $T_{world\_to\_proj}$ are also changing. Choosing one pair of the matrices in one position to solve equations (14) to (16) will induce random error.

(2) Measurement accuracy and robustness is low. For stereo SL system, most of the 3D points is simultaneously observed by the left camera, the right camera and the projector. To make the best use of the observed information from triple views and improve the measurement accuracy and robustness, the imaging constraint of another camera can be added on the basis of the classical SL system model.

In order to overcome above limitations, the projector coordinate is used as the measuring coordinate and the stereo SL system model is proposed, as shown in figure 5, which can be expressed as:

$$Z_c^L \begin{bmatrix} u_c^L & v_c^L & 1 \end{bmatrix}^T = P_{camL} \bullet T_{proj\_to\_camL} \bullet \begin{bmatrix} X_p & Y_p & Z_p & 1 \end{bmatrix}^T, \quad (17)$$

$$Z_p \begin{bmatrix} u_p & v_p & 1 \end{bmatrix}^T = P_{proj} \bullet \begin{bmatrix} X_p & Y_p & Z_p & 1 \end{bmatrix}^T, \quad (18)$$

$$Z_c^R \begin{bmatrix} u_c^R & v_c^R & 1 \end{bmatrix}^T = P_{camR} \bullet T_{proj\_to\_camR} \bullet \begin{bmatrix} X_p & Y_p & Z_p & 1 \end{bmatrix}^T, \quad (19)$$

$$u_p = \Phi / (2\pi f), \quad (20)$$

where P_{camL} and P_{camR} are the projection matrices of the left camera and the right camera, respectively, and Φ is the phase of point (u_c^L, v_c^L). $T_{proj\_to\_camL}$ and $T_{proj\_to\_camR}$ are the transformation matrices from the projector coordinate to the left and right cameras, respectively, which can be acquired by optimizing the linear equations as follows:

$$T_{proj\_to\_camL} \bullet T_{world\_to\_proj} = T_{world\_to\_camL}, \quad (21)$$

$$T_{proj\_to\_camR} \bullet T_{world\_to\_proj} = T_{world\_to\_camR}, \quad (22)$$

where $T_{world\_to\_camL}$, $T_{world\_to\_camR}$ and $T_{world\_to\_proj}$ at each position of the calibration board are known after the calibration of the stereo cameras and the projector. In the process of system calibration, the phase values at the corner points in the left and right unwrapped phase maps are not completely the same. Thus, the mean value is considered as the phase at the corner points in order to make the corner points in the left and right camera image plane correspond to the corner points in the projector plane. After the calibration of the stereo SL system, the projection matrices, P_{camL}, P_{camR} and P_{proj}, and the extrinsic matrices, $T_{proj\_to\_camL}$ and $T_{proj\_to\_camR}$, are obtained. Equations (17) to (20) provide 10 equations with 7 unknown parameters $(X_p, Y_p, Z_p, u_p, v_p, Z_c^L, Z_c^R)$ for each known pixel point (u_c^L, v_c^L) in the left image and its matching point (u_c^R, v_c^R) in the right image. By calculating a least square solution using triple-view geometry constraints, 3D point (X_p, Y_p, Z_p) can be obtained. It is worth noting that the intrinsic parameters of camera and projector might be slightly changed due to the self-heating induced image distorsion [30]. To address this problem, one strategy is to preheat the projector and camera for some time to make the system work in the heat-balance stage, during which the image distorsion would stop. Another strategy is to model the parameters drift by calibrating the camera and projector in different temperatures to obtain the relationship between the increasing temperature and image distorsion and acquire the thermal deformation parameters [31, 32]. And when performing 3D measurements, the thermal deformation parameters are utilized to rectify the projection parameters according to the increment of temperature.

3. Experiment

To verify the effectiveness of the proposed method, a high speed stereo SL system was developed, which is composed of two high speed CMOS cameras (Model: Ximea MQ013MG-ON) with a 12 mm focal length lens (Model: CHIOPT FA1201C) and one high-speed DLP projector (LightCrafter 4500) with an intrinsic resolution of 912×1140. The resolution of the camera is 1280×1024 and the CMOS sensor size is 1/2 inches. The synchronization between the cameras and the projector is achieved by the output trigger of the projector. The employed three-step sinusoidal fringe patterns are vertical and consist of 70 cycles. The speckle pattern contains 60000 speckles with a diameter of three pixels. The size of the image correlation window is 13×13 pixels.

3.1. 3D shape measurement

We first measured a static scene composed of three isolated objects to verify the ability of the proposed method in retrieving the absolute phase. The first captured fringe images from the left and right cameras are shown in figures 7(a) and 7(e), respectively. The captured speckle images of the left and right cameras are shown in figures. 7(b) and 7(f), respectively. The absolute phase maps of stereo images were retrieved using the developed method and are shown in figures. 7(c) and 7(g). Figures. 7(d) and 7(h) display a cross section (red dash line in figures. 7(c) and 7(g)) of each unwrapped phase map. As shown in figures. 7(d) and 7(h), the phase offset of each

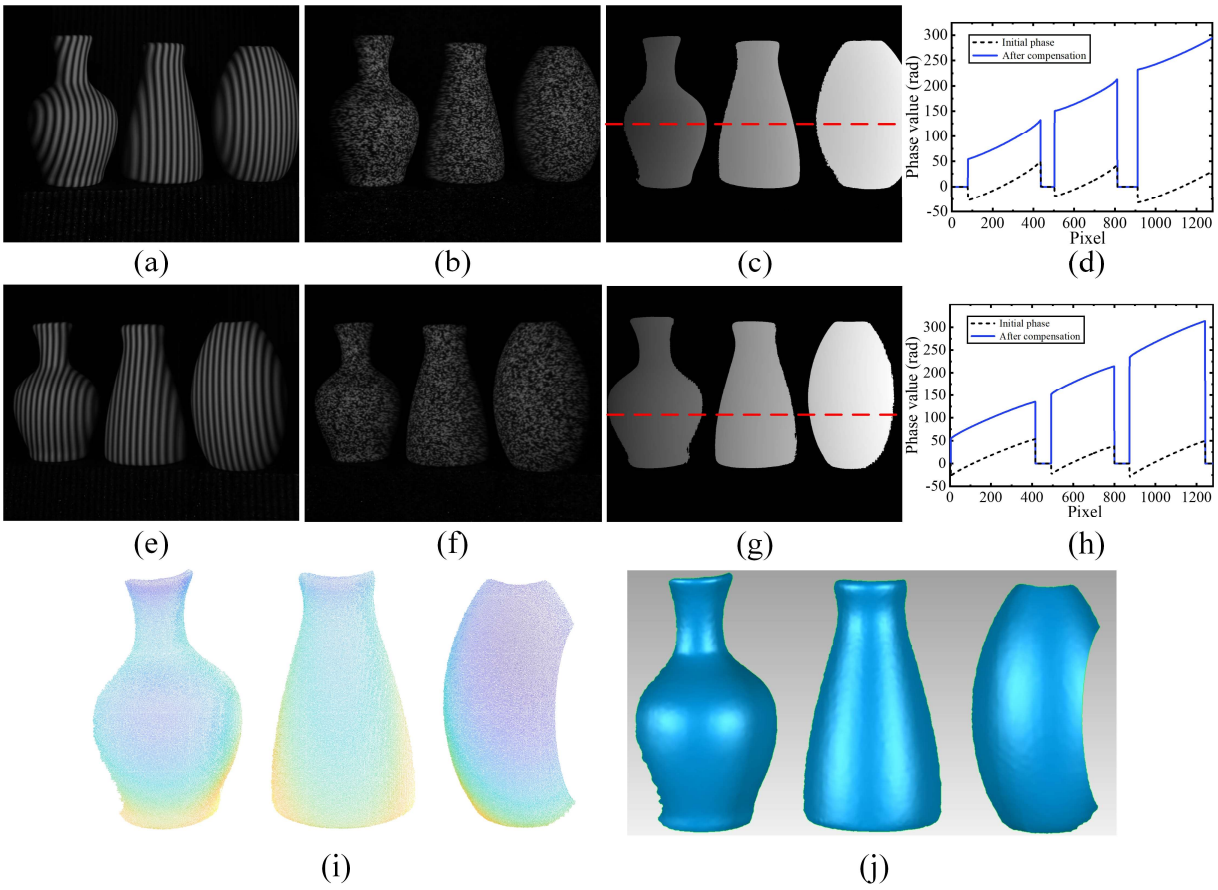

Figure 7. Measurement results of three isolated objects. (a) The first captured fringe image from left camera. (b) The last captured speckle image from left camera. (c) Unwrapped phase map from left camera. (d) One cross section (red dash line in (c)) of unwrapped phase map. (d)–(h) Corresponding images from right camera. (i) 3D point cloud. (j) 3D surface reconstruction result.

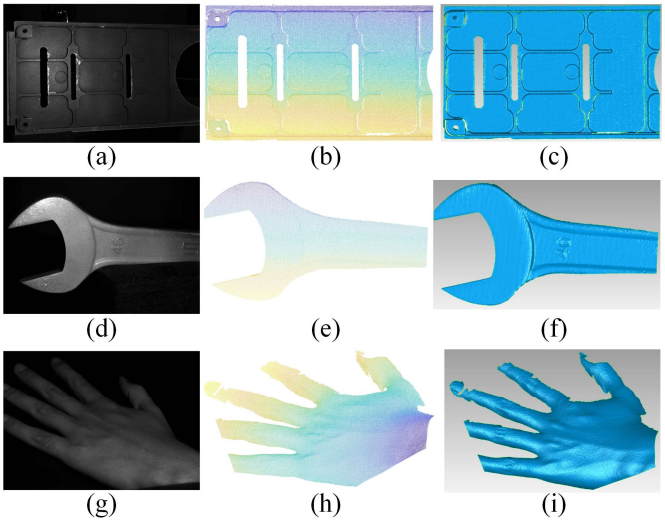

Figure 8. Measurement results of various objects. (a) Photograph of the casting part. (b) 3D point cloud of the casting part. (c) Surface reconstruction result of the casting part. (d)–(f) Corresponding images of the wrench. (g)–(i) Corresponding images of a hand.

isolated phase region in the initial phase map has been correctly compensated and the full-field phase distribution is continuous. Then the 3D data is calculated based on the proposed stereo SL system model and the 3D surface is also reconstructed. The 3D point cloud and surface reconstruction results are shown in figures. 7(g) and 7(f) and all the isolated objects have been reconstructed correctly, which indicates that the proposed method is capable of measuring multiple isolated objects.

In addition, we applied the proposed DIC-assisted phase-shifting method to various objects including a casting part, a wrench and a hand, as shown in figures 8(a), 8(d) and 8(g), respectively. Figures 8(b), 8(e) and 8(h) show the calculated 3D point clouds of these objects, respectively. Figures 8(c), 8(f) and 8(i) show the surface reconstruction results. Except for some regions that cannot be simultaneously captured by the stereo cameras and the projector, almost all the visible points were correctly reconstructed. The results of this experiment indicate that the proposed method is reliable in measuring the object with a complex surface.

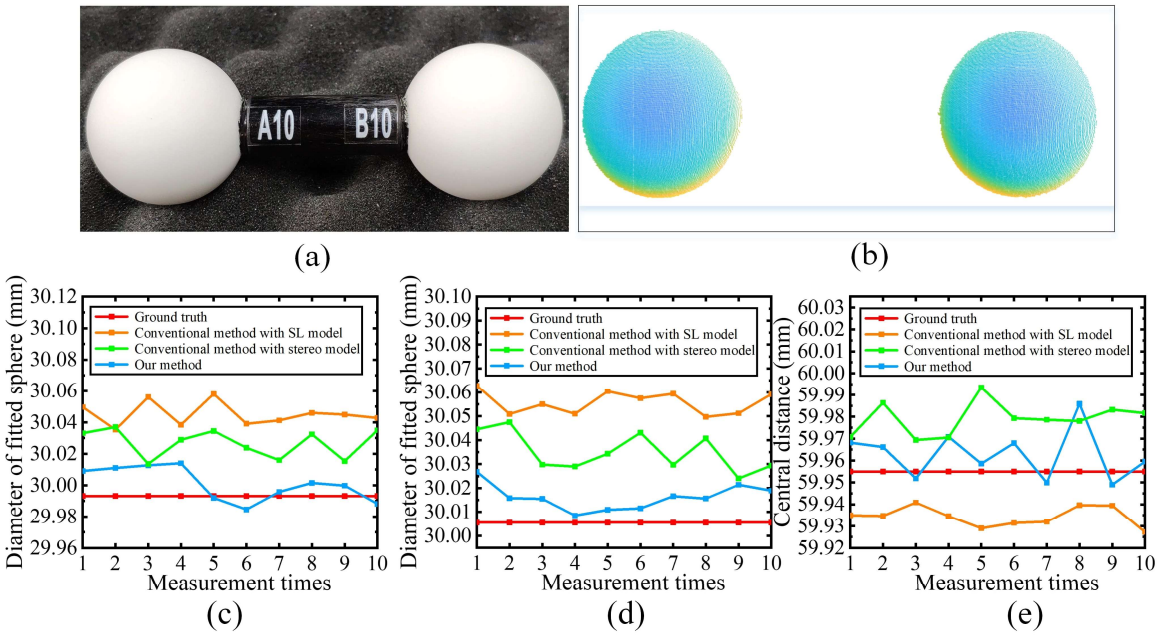

Figure 9. (a) Measured ceramic spheres. (b) 3D point cloud. (c)–(e) Measurement results of sphere A10, sphere B10 and central distance.

Table 1. Comparison of the MAE of the proposed method and the conventional methods (units: μm).

Method	MAE of the diameter of sphere A10	MAE of the diameter of sphere B10	MAE of the central distance
Our method	10.63	10.65	10.64
Conventional method with SL model	51.95	50.21	20.65
Conventional method with stereo model	33.75	29.70	24.13

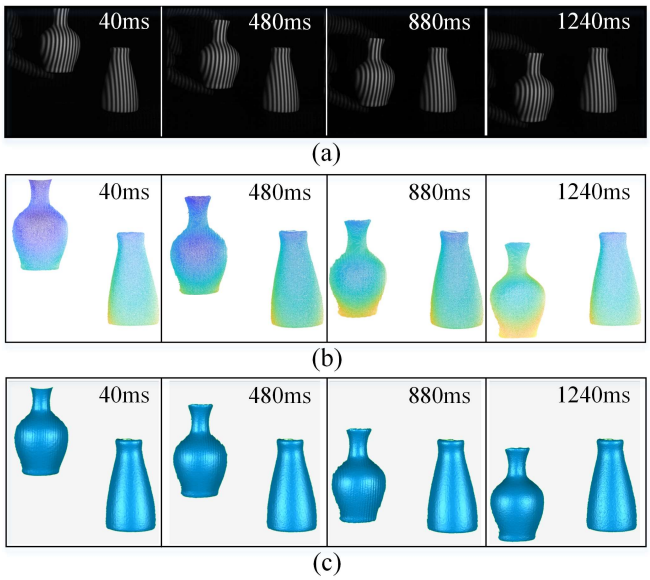

Figure 10. (a) Measurement results of dynamic objects. (a) Captured fringe images of dynamic scene in different times. (b) 3D point cloud. (c) 3D surface reconstruction result.

3.2. Accuracy evaluation

We tested the measurement accuracy of the proposed DIC-assisted phase-shifting method utilizing proposed stereo SL system model by comparing it with a conventional three-frequency four-step phase-shifting algorithm [15] utilizing SLsystem model and stereo vision model, respectively. In this experiment, two ceramic spheres, as shown in figure 9(a), with diameters of 29.9932 or 30.0055 mm and a central distance of 59.9550 mm were measured for 10 times from different views. Figure 9(b) shows one of the 10-time measured 3D point clouds. By fitting two spheres using the 3D point cloud, the diameters and central distance of these two spheres can be obtained. The measurement results of sphere A10, sphere B10 and central distance are shown in Figures 9(c)–(e), respectively.The mean absolute error (MAE) of the 10-time measured diameters and center distances using three methods are calculated and shown in Table 1. As can be seen from Table 1, the measurement accuracy of the proposed method can achieve a spatial resolution of 10 μm, which is more accurate than the conventional methods. The improvement of measurement accuracy is mainly due to the stereo SL system

model, which introduces an additional constraint of another camera and improves the precision of 3d data calculation. This experiment proves that the proposed method can perform high accuracy 3D shape measurements.

3.3. Dynamic measurement

To test the performance of the proposed method in dynamic measurement, a dynamic scene, as shown in figure 10(a), was measured by moving a vase (the left one) from top to bottom. During the movement, another static vase was placed alone on one side of the scene. The measurement system was working at a frequency of 120 Hz. Figure 10(a) shows the captured fringe images at different moments during the moving process. For this experiment, the moving process was firstly recorded followed by the calculation of the 3D data off-line. Figures 10(b) and 10(c) show the calculated 3D point clouds and surface reconstruction results of the dynamic scene at different moments. As can be seen from figure 10, the moving object and the static object were both reconstructed correctly with high-quality, which demonstrates that the capability of the proposed method in observing locomotive objects.

4. Discussion

The presented DIC-assisted phase shifting method based on proposed stereo SL model for 3D shape measurement in this paper has following advantages.

- *Robustness in absolute phase retrieval.* Several existing methods eliminate the phase ambiguity with local features embedded in the patterns or geometry constraints using pre-defined depth range of the objects, which decrease the robustness and practicability of structured-light system. Since DIC technique is utilized to calculate only a series of sparse stereo correspondence, the matching results and phase offsets can be determined reliably. Consequently, the absolute phase can be retrieved without using any embedded features or pre-defined depth range information.
- *High accuracy.* Benefitting from the stereo SL system model, which is proposed for the first time to our knowledge, more accurate 3D data calculated in the projector coordinates can be obtained by solving a least square solution using the triple-view information. The measurement accuracy can achieve a spatial resolution of 10 μm, which is superior to the related researches.
- *High-speed data acquisition.* Conventional multi-frequency methods project at least six patterns to acquire the unwrapped phase, and the proposed system can work at a frequency of 120Hz by only projecting four patterns.

Just like any other 3D measurement methods, the proposed DIC-assisted phase shifting method is not absolutely universal and indefective. The major limitation is:

- *Abrupt surfaces*. The proposed method faces challenges when measuring objects with abrupt spatial discontinuities, which is a common problem to all spatial phase unwrapping based methods. To reduce the impact of abrupt surfaces, a strategy is to decrease the number of fringes, which could sacrifice the measurement accuracy. How to address this challenge using more stereo constraint information will be another direction for the further investigation.

Despite of the limitation, the proposed method can perform accurate and dynamic 3D measurement without using any embedded features or pre-defined depth range information and can substantially benefit the 3D profilometry field and practical applications.

5. Conclusion

In this paper, a DIC-assisted phase-shifting method based on the proposed stereo structured-light system model is presented for accurate and dynamic 3D shape measurements. By projecting three-step phase shift patterns and one speckle pattern, the absolute phase map of captured stereo images can be retrieved correctly without requiring any embedded features or pre-defined information of the objects. To make the best use of the stereo camera and improve the measurement accuracy of SL system, the projector coordinate is used as the measuring coordinate and the stereo structured-light system model is proposed. The intrinsic and extrinsic parameters of the cameras and the projector can be obtained by one-time system calibration. By calculating a least square solution based on the proposed model, more accurate 3D data can be acquired. The experimental results show that the measurement accuracy of the proposed method can achieve a spatial resolution of 10 μm, which is obviously superior to conventional methods. In addition, the proposed method can be applied to the measurement for dynamic scenes due to its advantage of projecting less patterns. According to the dynamic measurement results, there are still motion ripples when the measuring rapidly moving objects. In the future, our work will focus on the compensation of motion-induced phase error to further improve the measurement performance in dynamic scenes.

Acknowledgements

The authors would like to thank the support by National Science Fund for Excellent Young Scholars (51722509); National Key Research and Development Program of China (2017YFB1104700); Program for Science and Technology Innovation Group of Shaanxi Province (2019TD-011); Key Research and Development Program of Shaanxi Province (2020ZDLGY04-02).

References

[1] Chen F, Brown GM and Song M 2000 Overview of three-dimensional shape measurement using optical methods *Opt. Eng.* **39** 10–22.

[2] Park H S, Park J S and Oh B K 2017 Vision-based stress estimation model for steel frame structures with rigid links. *Meas. Sci. Technol.* **28**(7) 075104.

[3] Kieu H, Pan T, Wang Z, Le M, Nguyen H and Vo M 2014 Accurate 3D shape measurement of multiple separate objects with stereo vision. *Meas. Sci. Technol.* **25**(3) 035401.

[4] Yu L, Fu X, Xu H and Fei S 2020 High-precision camera pose estimation and optimization in a large-scene 3D reconstruction system. *Meas. Sci. Technol.* **31** 085401.

[5] Dorrington A A, Cree M J, Payne A D, Conroy R M and Carnegie D A 2007 Achieving sub-millimetre precision with a solid-state full-field heterodyning range imaging camera. *Meas. Sci. Technol.* **18**(9) 2809–2816.

[6] Yang S, Shi X, Zhang G and Lv C 2018 A Dual-Platform Laser Scanner for 3D Reconstruction of Dental Pieces. *Engineering* **4**(6) 796–805.

[7] Der Jeught SV and Dirckx JJ 2016 Real-time structured light profilometry: a review. *Opt. Lasers Eng.* **87** 18–31.

[8] Zhang G, Yang S, Fluegge J and Bosse H 2020 Fiber optic white light interferometer for areal surface measurement. *Meas. Sci. Technol.* **31**(2) 025005.

[9] Schaffer M, Grosse M, Harendt B and Kowarschik R 2011 High-speed three-dimensional shape measurements of objects with laser speckles and acousto-optical deflection. *Opt. Lett.* **36**(16) 3097–3099

[10] Zhu J, Zhou P, Su X and You Z 2016 Accurate and fast 3D surface measurement with temporal-spatial binary encoding structured illumination. *Opt. Express* **24**(25) 28549–28560.

[11] Su X and Chen W 2001 Fourier transform profilometry: a review. *Opt. Lasers Eng.* **35**(5) 263–284.

[12] Pan B 2018 Digital image correlation for surface deformation measurement: historical developments, recent advances and future goals. *Meas. Sci. Technol.* **29**(8) 082001.

[13] Huang PS and Zhang S 2006 Fast three-step phase-shifting algorithm. *Appl. Opt.* **45**(21) 5086–5091.

[14] Su X and Chen W 2004 Reliability-guided phase unwrapping algorithm: a review. *Opt. Lasers Eng.* **42**(3) 245–261.

[15] Towers CE, Towers DP and Jones JD 2005 Absolute fringe order calculation using optimised multi-frequency selection in full-field profilometry. *Opt. Lasers Eng.* **43**(7) 788–800.

[16] Sansoni G, Carocci M and Rodella R 1999 Three-dimensional vision based on a combination of gray-code and phase-shift light projection: analysis and compensation of the systematic errors. *Appl. Opt.* **38** 6565.

[17] Cong P, Xiong Z, Zhang Y, Zhao S and Wu F 2015 Accurate Dynamic 3D Sensing With Fourier-Assisted Phase Shifting. *IEEE J. Sel. Top. Signal Process.* **9**(3) 396–408.

[18] Zhong K, Li Z, Shi Y, Wang C and Lei Y 2013 Fast phase measurement profilometry for arbitrary shape objects without phase unwrapping. *Opt. Lasers Eng.* **51**(11), 1213–1222.

[19] An Y, Zhang J and Zhang S 2016 Pixel-wise absolute phase unwrapping using geometric constraints of structured light system. *Opt. Express* **24**(16):18445–18459.

[20] Jiang C, Li B and Zhang S 2017 Pixel-by-pixel absolute phase retrieval using three phase-shifted fringe patterns without markers. *Opt. Lasers Eng.* **91** 232–241.

[21] Wu G, Wu Y, Li L and Liu F 2019 High-resolution few-pattern method for 3D optical measurement. *Opt. Lett.* **44**(14) 3602–3605.

[22] Feng S, Chen Q and Zuo C 2015 Graphics processing unit–assisted real-time three-dimensional measurement using speckle-embedded fringe. *Appl. Opt.* **54**(22) 6865.

[23] Lohry W, Chen V and Zhang S 2014 Absolute three-dimensional shape measurement using coded fringe patterns without phase unwrapping or projector calibration. *Opt. Express* **22**(2) 1287–1301.

[24] Yin W, Feng S, Tao T, Huang L, Trusiak M, Chen Q and Zuo C 2019 High-speed 3D shape measurement using the optimized composite fringe patterns and stereo-assisted structured light system. *Opt. Express* **27**(3) 2411–2431.

[25] Gai S, Da F and Dai X 2016 Novel 3D measurement system based on speckle and fringe pattern projection. *Opt. Express* **24**(16):17686–17697.

[26] Feng S, Chen Q, Zuo C and Asundi A 2017 Fast three-dimensional measurements for dynamic scenes with shiny surfaces. *Opt. Commun.* **382** 18–27.

[27] Lei H, Chang X, Wang F, Hu X and Hu, X 2015 A novel algorithm based on histogram processing of reliability for two-dimensional phase unwrapping. *Optik* **126**(18) 1640–1644.

[28] Zhang S and Yau S T 2007 Generic nonsinusoidal phase error correction for three-dimensional shape measurement using a digital video projector. *Appl. Opt.* **46**(1) 36–43.

[29] Zhang S and Huang PS 2006 Novel method for structured light system calibration. *Opt. Eng.* **45**(8) 083601.

[30] Ma S, Pang J and Ma Q 2012 The systematic error in digital image correlation induced by self-heating of a digital camera. *Meas. Sci. Technol.* **23** 025403.

[31] Handle H 2007 Analyzing the influences of camera warm-up effects on image acquisition. *In: Proceedings of the Asian Conference on Computer Vision.* **4844** 258–268.

[32] Ma S, Zhou S and Ma Q 2019 Image distortion of working digital camera induced by environmental temperature and camera self-heating. *Opt. Lasers Eng.* **115** 67–73.